

Quantum paraelectric behavior of pyrochlore PMN

S. Kamba,* D. Nuzhnyy, S. Denisov, S. Veljko, V. Bovtun, M. Savinov, and J. Petzelt
*Institute of Physics, Academy of Sciences of the Czech Republic,
v.v.i. Na Slovance 2, 182 21 Prague 8, Czech Republic*

M. Kalnberga and A. Sternberg
*Institute of Solid State Physics, University of Latvia, Kengaraga str. 8, Riga, Latvia
(Dated: May 27, 2019)*

Pb_{1.83}Mg_{0.29}Nb_{1.71}O_{6.39} (PMN) crystallizing in a cubic pyrochlore structure exhibits typical feature of quantum paraelectrics - its permittivity continuously increases on cooling and levels off below ~ 30 K without any signature of a structural phase transition. Broad-band dielectric spectra do not show any dielectric dispersion in the real part of permittivity up to 8.8 GHz. THz and infrared spectra reveal a polar optic soft mode which is responsible for the temperature dependence of the permittivity. The leveling-off of the permittivity at low temperatures obeys the Barrett formula and the fitted vibrational zero-point energy $\frac{1}{2}k_B T_1$ corresponds to the measured soft mode frequency. The number of observed infrared phonons exceeds that predicted from the factor-group analysis which indicates that the structure is at least locally non-cubic.

PACS numbers: 63.20.-e; 77.22.-d; 78.30.-j; 67.20.+k

I. INTRODUCTION

PbMg_{1/3}Nb_{2/3}O₃ crystallizing in the cubic perovskite structure is one of the most studied dielectrics as the typical representative of relaxor ferroelectrics. It exhibits a high ($\sim 10^4$) and strongly diffused peak in the temperature dependent permittivity whose position remarkably shifts from 245 K (at 100 Hz) to 320 K (at 1 GHz).^{1,2} Its crystal structure remains cubic down to liquid He temperatures. The peculiar dielectric properties are caused by a wide dielectric relaxation which broadens and slows down on cooling.³ The relaxation originates from the dynamics of polar clusters, which develop below the Burns temperature $T_d \cong 620$ K.⁴ The broad distribution of relaxation frequencies has its origin in random fields and random forces as a consequence of chemical disorder in the B site perovskite sites occupied by Mg²⁺ and Nb⁵⁺. The local ferroelectric instability in the polar clusters was indicated by an unstable polar optic phonon, which softens to T_d and hardens above T_d .^{5,6} Although the dielectric properties of perovskite PbMg_{1/3}Nb_{2/3}O₃ were intensively studied during the last fifty years, everything is still not completely understood, particularly the complex and broad dielectric dispersion.

The related compound Pb_{1.83}Mg_{0.29}Nb_{1.71}O_{6.39} (PMN) with a pyrochlore structure, which frequently grows in the perovskite PMN ceramics and thin films as a second phase and significantly deteriorates its dielectric properties, has been much less studied. The only report known to the authors was performed by Shrout and Swartz.⁷ They investigated the dielectric response up to 400 kHz down to liquid He temperatures and observed a diffuse maximum in the complex permittivity below 40 K. The crystal structure of the pyrochlore PMN single crystal (*Fd3m* space group) was determined in detail by Wakiya et al.⁸ High-frequency dielectric properties, including microwave, THz and infrared frequencies, have

not been investigated, although they would be useful for understanding the reported diffused and frequency dependent maximum of complex permittivity. The present report aims to fill this gap in the literature.

II. EXPERIMENTAL

Pb_{1.83}Mg_{0.29}Nb_{1.71}O_{6.39} pyrochlore ceramic samples were produced by solid state reaction of mixed oxide powders described in details in Refs.^{7,9} PbO (99.5%), Nb₂O₅ (99.5%) and MgO (97%) powders were mixed and sintered at 880 °C for 8 hours. The pyrochlore cubic structure was verified by the X-ray diffraction.

The dielectric response was investigated between 400 Hz and 1 MHz from 10 K to 730 K using an impedance analyzer HP 4192A. The TE_{0n1} composite dielectric resonator method¹⁰ and network analyzer Agilent E8364B was used for microwave measurements at 8.8 GHz in 100 - 350 K temperature interval. The cooling rate was 2 K/min.

Measurements at terahertz (THz) frequencies from 7 cm⁻¹ to 33 cm⁻¹ (0.2 - 1.0 THz) were performed in the transmission mode using a time-domain THz spectrometer based on an amplified Ti - sapphire femtosecond laser system. Two ZnTe crystal plates were used to generate (by optic rectification) and to detect (by electro-optic sampling) the THz pulses. Both the transmitted field amplitude and phase shift were simultaneously measured; this allows us to determine directly the complex dielectric response $\varepsilon^*(\omega)$. An Optistat CF cryostat with thin mylar windows (Oxford Inst.) was used for measurements down to 10 K.

Infrared (IR) reflectivity spectra were obtained using a Fourier transform IR spectrometer Bruker IFS 113v in the frequency range of 20 - 3000 cm⁻¹ (0.6 - 90 THz) at room temperature, at lower temperatures the

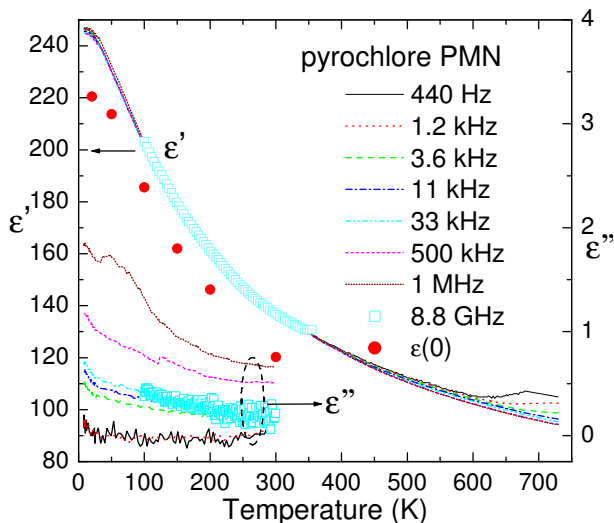


FIG. 1: (color online) Temperature dependence of the real ϵ' and imaginary ϵ'' part of complex permittivity in pyrochlore PMN ceramics at different frequencies. $\epsilon(0)$ means the sum of phonon and electronic contributions to the static permittivity, as obtained from the IR reflectivity and THz data fit. ϵ'' data are plotted only below 300 K, because its higher temperature values are influenced by the conductivity. Note the right scale for ϵ'' .

reduced spectral range up to 650 cm^{-1} only could be studied (transparency region of polyethylene windows in the cryostat). Pyroelectric deuterated triglicine sulfate detectors were used for the room temperature measurements, while more sensitive liquid-He cooled (1.5 K) Si bolometer was used for the low-temperature measurements. Polished disk-shaped samples with a diameter of 8 mm and thickness of ~ 2 mm were investigated.

III. RESULTS AND DISCUSSIONS

The temperature dependence of the real and imaginary parts of complex permittivity $\epsilon^* = \epsilon' - i\epsilon''$ at various frequencies is plotted in Fig. 1. One can see typical incipient ferroelectric behavior, i.e. increase in ϵ' on cooling and its noticeable saturation at low temperatures. It is important to stress that within the accuracy of measurements no frequency dispersion of ϵ' was observed between 400 Hz and 8.8 GHz at temperatures below 600 K. The small low-frequency dispersion above 600 K is caused by non-negligible conductivity of our sample. The pronounced $\epsilon'(T)$ dependence is therefore caused by the softening of an excitation above 10 GHz. To reveal it we measured the THz dielectric spectra (see Fig. 2) and IR reflectivity spectra (Fig. 3) below room temperature (RT). One can actually see very pronounced changes in the THz complex permittivity due to the polar phonon softening in the investigated range (see Fig. 2).

In order to obtain all phonon parameters as a function

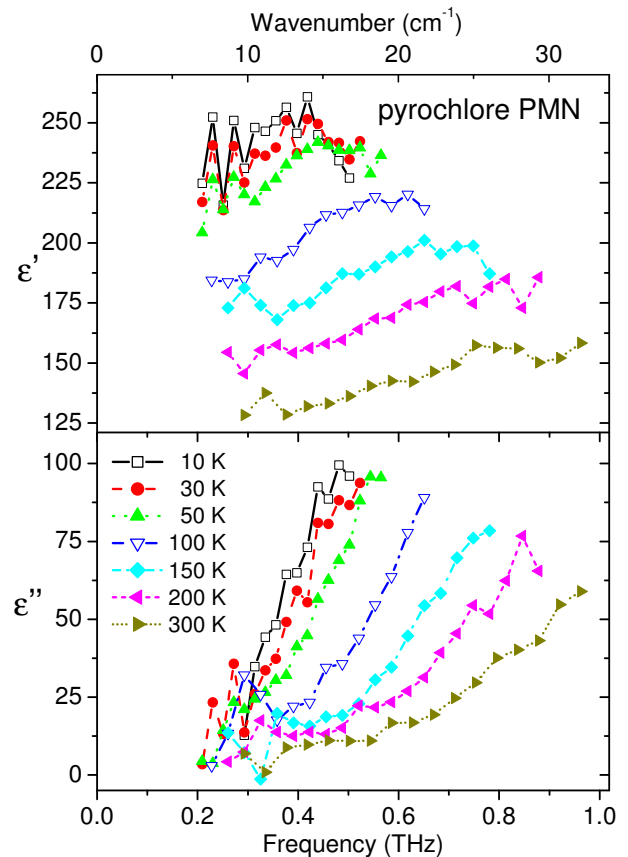


FIG. 2: (color online) THz dielectric spectra of the pyrochlore PMN at various temperatures. The soft mode frequency shift down into the THz range on cooling, therefore the sample becomes less transparent at low temperatures (the noise increases) and the accessible spectral range narrows on cooling. Two frequency scales (THz and cm^{-1}) are given.

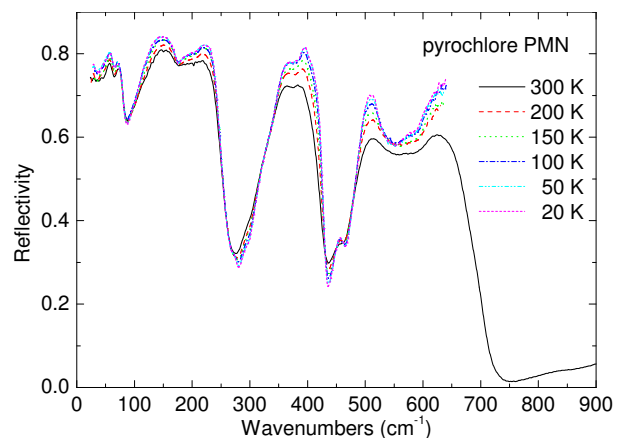


FIG. 3: (color online) IR reflectivity spectra of the pyrochlore PMN ceramics at various temperatures below RT. Low-temperature spectra were obtained only below 650 cm^{-1} (transparency range of the polyethylene windows in cryostat).

of temperature, IR and THz spectra were fitted simultaneously using the generalized-oscillator model with the factorized form of the complex permittivity:¹¹

$$\varepsilon^*(\omega) = \varepsilon_\infty \prod_j \frac{\omega_{LOj}^2 - \omega^2 + i\omega\gamma_{LOj}}{\omega_{TOj}^2 - \omega^2 + i\omega\gamma_{TOj}} \quad (1)$$

where ω_{TOj} and ω_{LOj} denotes the transverse and longitudinal frequency of the j -th polar phonon, respectively, and γ_{TOj} and γ_{LOj} denotes their corresponding damping constants. $\varepsilon^*(\omega)$ is related to the reflectivity $R(\omega)$ by

$$R(\omega) = \left| \frac{\sqrt{\varepsilon^*(\omega)} - 1}{\sqrt{\varepsilon^*(\omega)} + 1} \right|^2. \quad (2)$$

The high-frequency permittivity ε_∞ resulting from the electronic absorption processes was obtained from the room-temperature frequency-independent reflectivity tails above the phonon frequencies and was assumed to be temperature independent.

The real and imaginary parts of $\varepsilon^*(\omega)$ obtained from the fits to IR and THz spectra are shown in Fig. 4. Parameters of the fits performed at 300 and 20 K are summarized in Table I. One can see a higher number of observed modes at 20 K than at RT. This is due to the reduced phonon damping at low temperatures, which allows to resolve a higher number of modes, which are probably overlapping at RT. One can see in the $\varepsilon''(\omega)$ spectra of Fig. 4 (we remind that the frequencies of ε'' maxima roughly correspond to the phonon frequencies) that the most remarkable frequency shift with temperature exhibits the lowest frequency mode below 30 cm^{-1} , but also the mode near 130 cm^{-1} partially softens on cooling. The temperature dependence of the soft mode frequency ω_{SM} (left scale) and its dielectric strength $\Delta\varepsilon_{SM}$ are shown in Fig. 5. Mainly this mode causes an increase in ε' on cooling (see Fig. 1). In the case of uncoupled phonons the oscillator strength $f_j = \Delta\varepsilon_j \omega_{TOj}^2$ of each phonon is roughly temperature independent so that each softening of phonon frequency ω_{TOj} is connected with the increase of its dielectric strength $\Delta\varepsilon_j$ given by:¹¹

$$\Delta\varepsilon_j = \varepsilon_\infty \omega_{TOj}^{-2} \frac{\prod_k \omega_{LOk}^2 - \omega_{TOj}^2}{\prod_{k \neq j} \omega_{TOk}^2 - \omega_{TOj}^2}. \quad (3)$$

In our case the soft-mode oscillator strength f_{SM} is temperature dependent, it increases twice from $3.3 \cdot 10^4$ to $6.5 \cdot 10^4 \text{ cm}^{-2}$. This indicates that the soft mode is coupled with some higher frequency mode assuming that $\sum f_j = \text{const.}$ However, it is difficult to reveal with which mode is the soft mode coupled, because the oscillator strength of the most high-frequency modes is much higher than f_{SM} and relatively small changes (below the limit of our fitting accuracy) in these modes could explain the increase of the f_{SM} on cooling.

The static permittivity obtained from the fit of the IR reflectivity is defined as

$$\varepsilon(0) = \sum_j \Delta\varepsilon_j + \varepsilon_\infty \quad (4)$$

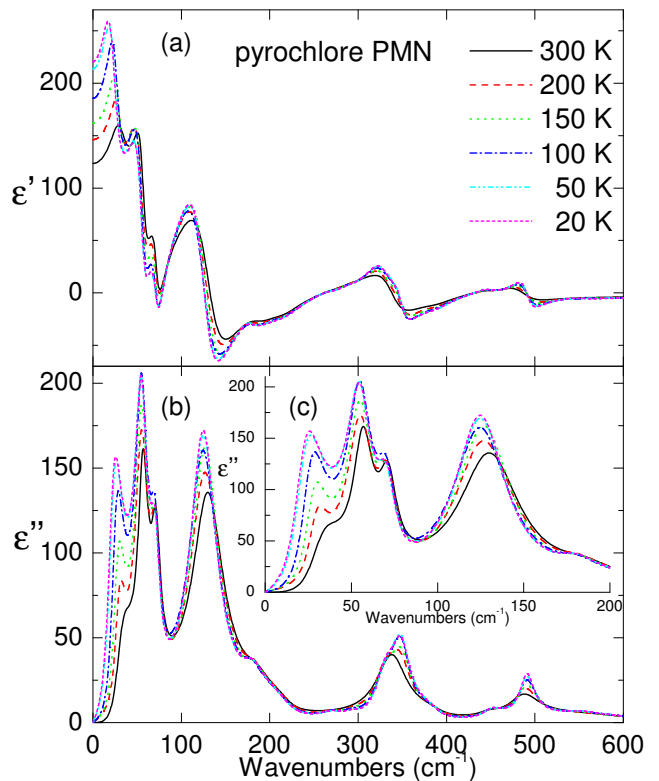


FIG. 4: (color online) Complex dielectric spectra from the fit to IR reflectivity and THz dielectric spectra at various temperatures. To see better the mode softening, $\varepsilon''(\omega)$ in inset the spectra are shown in the spectral range below 200 cm^{-1} .

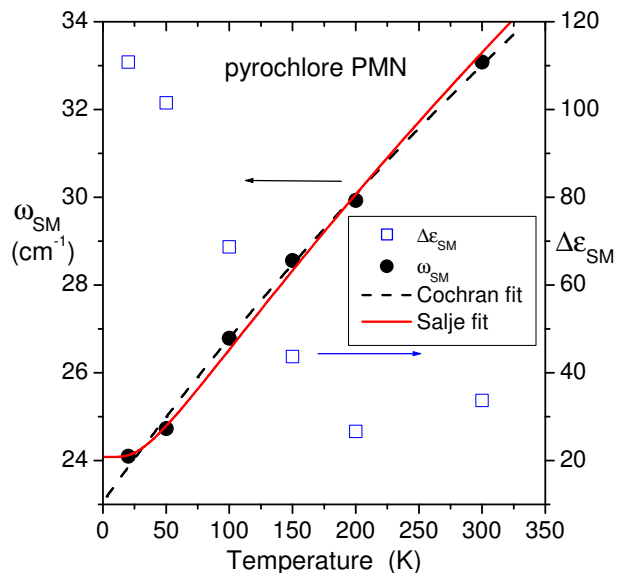


FIG. 5: (color online) Temperature dependence of the low-frequency soft mode ω_{SM} (left scale) and its dielectric strength $\Delta\varepsilon_{SM}$ (right scale). Dashed black line and solid red line show the results of the Cochran and Salje fit, respectively (see the text).

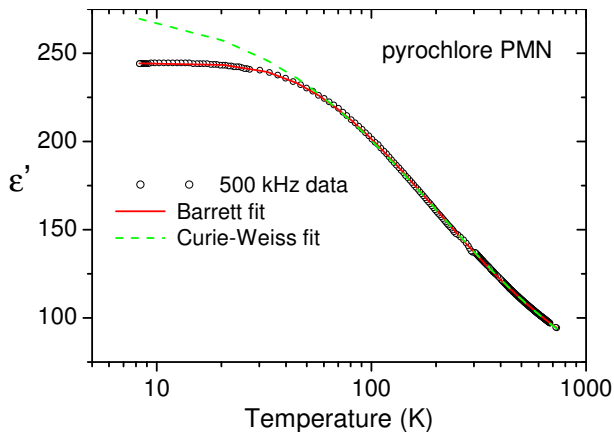


FIG. 6: (color online) The temperature dependence of the experimental permittivity at 500 kHz and result of the Curie-Weiss fit (dashed green line) and the fit with Barrett formula (red solid line).

and is plotted in Fig. 1 in red solid dots. The values of $\varepsilon(0)$ are slightly lower (by about 20) than the experimental values obtained at and below the microwave range. However, we think that the disagreement is more due to the experimental inaccuracy than due to real dielectric dispersion above the GHz range. So we conclude that the temperature dependence of the permittivity below 10 GHz in Fig. 1 is essentially due to anomalous polar phonons.

The temperature dependence of the lowest-mode frequency below 35 cm^{-1} was fitted with the Cochran law

$$\omega_{SM} = \sqrt{A(T - T_{cr})} \quad (5)$$

where A is a constant and T_{cr} is the critical softening temperature. From the fit we obtained $A = 1.86 \text{ cm}^{-2} \text{ K}^{-1}$ and $T_{cr} = -285 \text{ K}$. Therefore, pyrochlore PMN tends to the ferroelectric instability at negative temperatures.

Theoretical critical temperature can be obtained also from the fit of the temperature dependence of permittivity $\varepsilon(T)$, which (for classical paraelectrics) should follow the Curie-Weiss law

$$\varepsilon' = \varepsilon_{cw\infty} + \frac{C}{T - T_{cw}}. \quad (6)$$

The result of the Curie-Weiss fit is shown in Fig. 6 in dashed line with the following fit parameters: $\varepsilon_{cw\infty} = 43$, Curie-Weiss constant $C = 47800 \text{ K}$ and critical temperature $T_{cw} = -202 \text{ K}$. The Cochran critical temperature $T_{cr} = -285 \text{ K}$ is lower than the Curie-Weiss critical temperature T_{cw} , but if we consider that the extrapolated critical temperatures lie far below the investigated temperature range, the agreement between both values is reasonable.

The Curie-Weiss fit in Fig. 6 deviates from the experimental data below $\sim 50 \text{ K}$, because $\varepsilon'(T)$ levels off at low temperatures. Similar behavior was observed in

incipient ferroelectrics like SrTiO_3 , KTaO_3 or CaTiO_3 where the polar soft mode is also responsible for the observed $\varepsilon'(T)$.^{12,13,14} The soft mode does not soften completely, it levels off at low temperatures (typically below 30 K), mainly due to zero-temperature vibrations of light oxygen ions, which prevents the formation of long-range ferroelectric order and therefore the permittivity saturates at low temperatures. It is due to this phenomenon the incipient ferroelectrics are also called quantum paraelectrics.

The leveling-off of the low-temperature permittivity in incipient ferroelectrics was explained by Barrett¹⁵ already in the beginning of 1950's. He derived the formula

$$\varepsilon'(T) = \frac{M}{\frac{T_1}{2} \coth\left(\frac{T_1}{2T}\right) - T_0} + \varepsilon_{B\infty}, \quad (7)$$

where M is the constant, T_1 is the temperature, below which the quantum fluctuations start to play a role ($\frac{1}{2}k_B T_1$ is the zero-point vibration energy¹⁷) and $\varepsilon_{B\infty}$ marks the temperature independent part of the permittivity (this term was neglected in Ref.¹⁵, because it was very small in comparison to huge low-temperature ε' in SrTiO_3 and KTaO_3). Our use of the the Barrett formula in Eq. 7 for fitting of $\varepsilon'(T)$ yields very good agreement with the experimental data (see Fig. 6). We found $M = 4.2 \times 10^4 \text{ K}$, $T_1 = 95.8 \text{ K}$, $T_0 = -4 \times 10^{-3} \pm 1 \times 10^{-5} \text{ K}$ (we stress that $T_0 \neq 0$) and $\varepsilon_{B\infty} = 47$. For $T \gg T_1$, $\frac{1}{2}T_1 \coth\left(\frac{T_1}{2T}\right)$ asymptotically approaches T and Eq. 7 becomes a Curie-Weiss law. Therefore also $\varepsilon_{B\infty} = 47$ is close to $\varepsilon_{CW\infty} = 43$. It is worth to note that the zero point vibration frequency $\frac{1}{2}k_B T_1 = 1 \text{ THz}$ agrees perfectly with the soft mode frequency at RT (see Fig. 5). Note also that the T_1 parameter as well as the soft-mode frequency in the pyrochlore PMN qualitatively agree with analogous parameters obtained for SrTiO_3 and $\text{SrTi}^{18}\text{O}_3$, although the values of permittivity in these materials are two orders of magnitude higher,^{15,16} which is the consequence of different M parameters.

In the only published dielectric data below 400 kHz Shroud and Swartz⁷ observed similar essentially dispersionless increase in ε' on cooling down to 50 K as we did in Fig. 1. We believe that the small dispersion below 50 K and small decrease in ε' below $\sim 30 \text{ K}$ observed by Shroud and Swartz⁷ could be due to some defects (e.g. vacancies) in the crystal lattice of pyrochlore $\text{Pb}_{1.83}\text{Mg}_{0.29}\text{Nb}_{1.71}\text{O}_{6.39}$, which is substantially non-stoichiometric.

It is clear that the soft mode frequency cannot follow the Cochran law (Eq. 5) in the case of low-temperature quantum fluctuations. The correct low-temperature dependence was suggested by Salje¹⁷

$$\omega_{SM}^2 = DT_1 \left[\coth \frac{T_1}{2T} - \frac{T_1}{2T_0} \right], \quad (8)$$

where D is a fitting constant (note we slightly modified the Salje formula from Ref.¹⁷). Result of the fit with Salje formula is shown by solid line in Fig. 5 where one

TABLE I: Parameters of the polar phonon modes in the pyrochlore PMN obtained from the fit of IR and THz spectra at 20 and 300 K. Frequencies ω_{TOj} , ω_{LOj} and dampings γ_{TOj} , γ_{LOj} of modes are in cm^{-1} , $\Delta\varepsilon_j$ is dimensionless, $\varepsilon_\infty=5.87$.

No	20 K					300 K				
	ω_{TOi}	γ_{TOj}	ω_{LOj}	γ_{LOj}	$\Delta\varepsilon_j$	ω_{TOj}	γ_{TOj}	ω_{LOj}	γ_{LOj}	$\Delta\varepsilon_j$
1	24.1	19.4	32.5	31.5	110.8	33.2	22.6	37.7	30.5	33.7
2	55.8	16.1	63.9	17.7	36.6	56.9	13.5	63.2	16.9	23.9
3	71.7	13.4	80.1	14.5	12.0	71.9	12.3	79.7	18.1	10.8
4	125.9	36.1	175.8	28.4	46.1	131.9	42.9	182.3	40.6	40.8
5	179.9	28.0	212.0	68.7	1.8	186.7	36.2	215.3	56.3	1.6
6	216.7	49.2	257.3	23.2	0.8	217.6	41.6	260.1	40.2	0.4
7	271.2	26.0	277.3	22.0	0.26					
8	293.5	23.7	296.0	22.0	0.2					
9	329.7	29.5	339.8	30.7	0.3					
10	348.9	23.7	388.1	49.2	2.0	338.8	41.1	383.5	48.9	4.3
11	389.1	36.6	429.5	20.6	0.06	386.5	40.8	427.7	32.4	0.2
12	449.6	28.1	464.1	33.6	0.3	448.4	31.7	456.3	35.0	0.2
13	490.9	19.9	547.6	59.5	0.9	486.3	41.9	530.7	116.5	1.0
14	547.8	43.4	551.2	55.6	0.001	553.1	120	586.1	120.4	0.4
15	562.6	44.8	575.1	70.7	0.9					
16	598.9	70.5	703.6	46.8	0.4	602.6	104.9	703.6	47.6	0.3
17	862.7	80.1	863.0	69.1	0.002	862.7	80.1	863	69.1	0.002

can clearly see the leveling-off of the soft-mode frequency at low temperatures. The fitting parameters are the following: $D = 1.04 \text{ cm}^{-2}\text{K}^{-1}$, $T_1 = 95.8 \text{ K}$ and $T_0 = -10 \text{ K}$. The fit parameters can be significantly improved, if we would have more points in Fig. 5 especially at low temperatures below 50 K. Nevertheless, one can see reasonable agreement of both Cochran and Salje fits above 50 K.

Let us compare the IR reflectivity spectra of pyrochlore PMN (see Fig. 3) with those of perovskite PMN. The latter was first published by Burns and Dacol⁴ together with the temperature dependence of the optical index of refraction $n(T)$, which shows deviation from the linear dependence below $\sim 600 \text{ K}$. They explained unusual $n(T)$ dependence by formation of polar nanoregions. Surprisingly, the published IR spectrum of the perovskite sample⁴ corresponds to our pyrochlore spectrum in Fig. 3. In later papers of other authors (Refs.^{18,19,20,21}) the mutually similar (but different than Burns and Dacol's spectra⁴) IR reflectivity spectra of perovskite PMN consisted of three distinct reflection bands typical for all cubic perovskite oxides. It appears that the IR spectrum by Burns and Dacol⁴ belongs in reality to pyrochlore PMN. The rest of their data ($n(T)$ and $P(T)$) were obviously obtained on perovskite PMN, because the peculiarities near the Burns temperature in the perovskite PMN were later confirmed in many experiments.

It is of interest to compare the number of observed polar modes in reflectivity spectra with the prediction of factor-group analysis: pyrochlore PMN crystallizes in $Fd3m$ space group with 8 formula units per conventional unit cell,⁸ i.e. 2 formula units per primitive unit cell. This means that on the whole, 66 lattice vibrational

branches are expected. Pb ions are in 16d positions while Mg and Nb ions are in 16c positions⁸, both sites having D_{3d} symmetry, while the O cations are in positions 48f and 8b of C_{2v}^d and T_d symmetry, respectively. The mode symmetries and their activities in IR and Raman spectra can be obtained using standard tables²² with the following result for the Γ -point of the Brillouin zone (factor-group analysis):

$$\begin{aligned} \Gamma_{Fd3m} = & 3A_{2u}(-) + 3E_u(-) + 8F_{1u}(x) + 4F_{2u} \\ & + 4F_{2g}(xy, yz, xz) + A_{1g}(x^2, y^2, z^2) \\ & + E_g(x^2 + y^2 - 2z^2, \sqrt{3}x^2 - \sqrt{3}y^2) + 2F_{1g}. \end{aligned} \quad (9)$$

It means that after subtraction of $1F_{1u}$ acoustic mode, $7F_{1u}$ modes should be IR active, $4F_{2g}$, $1A_{1g}$ and $1E_g$ should be Raman active, the rest of modes being silent. Table I shows that the fit of IR spectra required 17 modes, much more than expected. The analysis in Eq. 9 assumes one effective ion in 16c positions instead of statistically distributed Mg and Nb ions. Since the ions strongly differ in the mass, one could expect splitting of modes in which these ions take part. If we take into account different Mg and Nb vibrations, the factor group analysis yields:

$$\begin{aligned} \Gamma_{Fd3m} = & 4A_{2u}(-) + 4E_u(-) + 10F_{1u}(x) + 5F_{2u} \\ & + 4F_{2g}(xy, yz, xz) + A_{1g}(x^2, y^2, z^2) \\ & + E_g(x^2 + y^2 - 2z^2, \sqrt{3}x^2 - \sqrt{3}y^2) + 2F_{1g}. \end{aligned} \quad (10)$$

In this case 9 polar F_{1u} modes are expected, which is still less than 17 modes observed at low temperature (see Table I). If we assume that the Pb cations and some of the oxygen anions are dynamically disordered among more

equivalent positions with the average structure remaining cubic like in isostructural $\text{Bi}_{1.5}\text{ZnNb}_{1.5}\text{O}_7$,²³ then 14 modes are IR active,²⁴ close to our experimental result.

This problem with the excess IR active modes is also known in the perovskite PMN, where only $3F_{1u}$ polar modes are allowed, although 7 modes were observed.^{20,21} The excess modes in the perovskite PMN were explained by polar clusters, which locally break the cubic symmetry into a rhombohedral one. In the case of pyrochlore structure similar local symmetry breaking, if present, should probably be non-polar, because there is no indication for the existence of polar clusters. No dielectric dispersion was observed below the polar phonon range, in contrast to PMN perovskite, where the huge dielectric dispersion appears just due to polar cluster dynamics.^{1,2,3} Nonetheless, it is also known for example that 38 IR active modes are allowed²⁵ in nonpolar orthorhombic pyrochlore structure. Therefore it appears that new structural studies of pyrochlore PMN are needed to detect either a dynamical disorder of some atoms in the lattice or a non-cubic crystal symmetry.

IV. CONCLUSION

Our dielectric studies of pyrochlore PMN revealed quantum paraelectric behavior, i.e. the permittivity in-

creases on cooling following the Barrett formula in the whole investigated temperature range. The permittivity shows no dispersion up to the microwave range and its temperature dependence can be explained by the softening of polar optic modes. The zero-point vibrational energy $\frac{1}{2}k_B T_1 = 1$ THz obtained from the Barrett formula corresponds very well with the soft mode frequency observed near 30 cm^{-1} . Our IR spectrum of pyrochlore PMN corresponds to IR spectrum by Burns and Dacol⁴, whose paper concerns the perovskite PMN. By comparing it with later results,^{18,19,20,21} it becomes clear that Burns and Dacol published by mistake the IR spectrum of the pyrochlore PMN. Since the IR experiment revealed more modes than expected from the factor-group analysis, we suggest that the structure should have at least locally lower symmetry than cubic.

Acknowledgments

The work has been supported by the Grant Agency of the Czech Republic (Project No. 202/06/0403) and AVOZ10100520.

-
- * Electronic address: kamba@fzu.cz
- ¹ V. Bovtun, S. Kamba, A. Pashkin, M. Savinov, P. Samoukhina, J. Petzelt, *Ferroelectrics*, **298**, 23 (2004).
 - ² V. Bovtun, S. Veljko, S. Kamba, J. Petzelt, S. Varkhrushev, Y. Yakymenko, K. Brinkman, and N. Setter, *J. Eur. Ceram. Soc.* **26**, 2867 (2006).
 - ³ D. Viehland, M. Wuttig, and L.E. Cross, *Ferroelectrics* **120**, 71 (1991).
 - ⁴ G. Burns and F. H. Dacol, *Solid State Commun.* **48**, 853 (1983).
 - ⁵ S. Wakimoto, C. Stock, Z.-G. Ye, W. Chen, P. M. Gehring, and G. Shirane, *Phys. Rev. B* **66**, 224102 (2002).
 - ⁶ S. Kamba, M. Kempa, V. Bovtun, J. Petzelt, K. Brinkman, and N. Setter, *J. Phys.: Condens. Matter* **17** 3965 (2005).
 - ⁷ T. R. Shroud and S. L. Swartz, *Mat. Res. Bull.* **18**, 663 (1983).
 - ⁸ N. Wakiya, A. Saiki, N. Ishizawa, K. Shinozaki, and N. Mizutani, *Mat. Res. Bull.* **28**, 137 (1993).
 - ⁹ A. Mergen and W.E. Lee, *J. Eur. Ceram. Soc.* **17**, 1033 (1997).
 - ¹⁰ J. Krupka, T. Zychowicz, V. Bovtun, S. Veljko, *IEEE Trans. UFFC* **53**, 1883 (2006).
 - ¹¹ F. Gervais, in *Infrared and Millimeter Waves*, vol. 8, ed. K. J. Button (New York: Academic) chapter 7, p. 279.
 - ¹² J. Petzelt, G.V. Kozlov, and A.A. Volkov, *Ferroelectrics* **73**, 101 (1987).
 - ¹³ G. A. Samara, *Solid State Physics, Advances in Research and Applications*, Vol. 56. San Diego: Academic Press, pp. 240-458 (2001) and references therein.
 - ¹⁴ J. Petzelt et al. *Phys. Rev. B* **64**, 184111 (2001).
 - ¹⁵ J.H. Barrett, *Phys. Rev.* **86**, 118 (1952).
 - ¹⁶ C. Filipic and A. Levstik, *Phys. Rev. B* **73**, 092104 (2006).
 - ¹⁷ E.K.H. Salje, B. Wruck, and H. Thomas, *Z. Phys. B: Condens. Matter* **82**, 399 (1991).
 - ¹⁸ A. A. Karamyan, *Sov. Phys. Solid State* **18**, 1861 (1977).
 - ¹⁹ I. M. Reaney, J. Petzelt, V. V. Voitsekhovskii, F. Chu, and N. Setter, *J. Appl. Phys.* **76**, 2086 (1994).
 - ²⁰ S.A. Prosandeev, E. Cockayne, B.P. Burton, S. Kamba, J. Petzelt, Yu. Yuzyuk, R.S. Katiyar, and S.B. Vakhruшев, *Phys. Rev. B* **70**, 134110 (2004).
 - ²¹ J. Hlinka, T. Ostapchuk, D. Noujni, S. Kamba, and J. Petzelt, *Phys. Rev. Lett.* **96**, 027601 (2006).
 - ²² D.L. Rousseau, R.P. Bauman, and S.P.S. Porto, *J. Raman Spectr.* **10**, 253 (1981).
 - ²³ I. Levin, T.G. Amos, J.C. Nino, T.A. Vanderah, C.A. Randall, and M.T. Lanagan, *J. Sol. State Chem.*, **168**, 69 (2002).
 - ²⁴ S. Kamba, V. Porokhonsky, A. Pashkin, V. Bovtun, and J. Petzelt, *Phys. Rev. B* **66**, 054106 (2002).
 - ²⁵ E. Buixaderas, S. Kamba, J. Petzelt, M. Savinov, and N.N. Kolpakova, *Eur. Phys. J. B* **19**, 9 (2001).